

# Learning to Control and Coordinate Hybrid Traffic Through Robot Vehicles at Complex and Unsignalized Intersections

Dawei Wang,<sup>1</sup> Weizi Li,<sup>2</sup> Lei Zhu,<sup>3</sup> Jia Pan<sup>1</sup>

<sup>1</sup>The University of Hong Kong

<sup>2</sup>The University of Memphis

<sup>3</sup>The University of North Carolina at Charlotte

## Abstract

Intersections are essential road infrastructures for traffic in modern metropolises; however, they can also be the bottleneck of traffic flows due to traffic incidents or the absence of traffic coordination mechanisms such as traffic lights. Thus, various control and coordination mechanisms that are beyond traditional control methods have been proposed to improve the efficiency of intersection traffic. Amongst these methods, the control of foreseeable hybrid traffic that consists of human-driven vehicles (HVs) and robot vehicles (RVs) has recently emerged. We propose a decentralized reinforcement learning approach for the control and coordination of hybrid traffic at real-world, complex intersections—a topic that has not been previously explored. Comprehensive experiments are conducted to show the effectiveness of our approach. In particular, we show that using 5% RVs, we can prevent congestion formation inside the intersection under the actual traffic demand of 700 vehicles per hour. In contrast, without RVs, congestion starts to develop when the traffic demand reaches as low as 200 vehicles per hour. Further performance gains (reduced waiting time of vehicles at the intersection) are obtained as the RV penetration rate increases. When there exist more than 50% RVs in traffic, our method starts to outperform traffic signals on the average waiting time of all vehicles at the intersection.

Our method is also robust against both blackout events and sudden RV percentage drops, and enjoys excellent generalizability, which is illustrated by its successful deployment in two unseen intersections.

## 1 Introduction

Uninterrupted traffic flows are the beating heart of cities. They are not only the driving force for socio-economic development but also an assurance for essential supplies' delivery to the

populace during emergent events. However, even with existing traffic control and management methods (such as traffic signals, ramp meters, street signs, and tolls) working at their full capacity, traffic delays and congestion are still a worldwide problem causing more than \$100 billion in external costs annually (1). Given that urbanization and motorization are projected to continue rising in the decades to come (2, 3), there is an immediate need for better design/management of our traffic systems.

Traffic is an interplay between vehicles and road infrastructure. Contemporary urban road networks largely consist of linearly-coupled road segments connected with intersections. The key to this design's functionality is the *intersection*, where traffic flow from different directions can interchange and disperse. Any incident at the intersection can block traffic on all connecting roads and cause traffic spillback over further upstream roads. It is not uncommon to observe an entire city's traffic becoming paralyzed because of the breakdown of major intersections. Unfortunately, intersections are prone to traffic incidents due to their varied (and potentially) complex topology and conflicting traffic streams. In the U.S., nearly half of all crashes take place at intersections (4). Additionally, extreme weather and energy shortages can take down our power grids causing the main intersection control method, traffic signals, to be absent for days, if not weeks. This leaves traffic stranded and bound to congest (5–7). This leaves us with the question: *how to ensure traffic flows uninterrupted at intersections?*

While exhaustive transport policies and control methods exist to contain traffic delays and congestion, technological advancements such as connected and autonomous vehicles (CAVs) offer us new opportunities. Recent studies (8, 9) have demonstrated the possibilities of using self-driving robot vehicles (RVs) to enhance traffic throughput at intersections; however, these studies assume that all vehicles present are mutually connected and centrally controlled—a condition that may not be realized in the near future. The adoption of vehicles with different levels of autonomy has been and will continue to be *gradual*. A mixture of human-driven ve-

hicles (HVs) and RVs, i.e., hybrid traffic, will long be experienced before the advent of fully autonomous transportation systems. Although hybrid traffic can be much more challenging to model and control compared to 100% RVs (considering the diversity and suboptimality of the human drivers’ behaviors), we may still be able to regulate it by first algorithmically determining the behaviors of the RVs and then using them to influence nearby HVs (10). Existing studies have demonstrated the potential of this hybrid system’s control in scenarios such as ring roads, figure-eight roads (10), highway bottleneck and merge (11, 12), two-way intersections (13), and roundabouts (14). However, most of these scenarios do not embed real-world complexity, and the number of vehicles that can potentially be in conflict is small.

In this research, we study the control and coordination of hybrid traffic at intersections. Given the importance of intersections, various traffic control mechanisms have been developed (15) with three approaches being the most prominent.

- Traffic signal control (16–18): a well-studied topic. Nevertheless, as we mentioned before, traffic lights are vulnerable to extreme conditions, and thus cannot guarantee uninterrupted traffic flows at intersections.
- Autonomous Intersection Management Systems (AIMS) (19, 20): a robust approach even during emergent events. However, this approach assumes all vehicles are centrally controlled and thus is not applicable to hybrid traffic.
- Reinforcement learning (RL). RL has shown great potential in high-dimensional, multi-agent control tasks (21–25) in recent years. It is a promising tool for hybrid traffic control because its model-free design copes with the absence of effective models for hybrid traffic. To date, most successful examples of hybrid traffic control (including the studies we mentioned before (10–14)) take this approach (26).

While significant progress has been made, none of the above-mentioned studies addresses *hy-*

brid traffic at real-world, complex intersections where a large number of vehicles can potentially be in conflict under actual traffic demands. Our study subjects include four real-world intersections, along with their actual traffic data, from Colorado Springs, CO, USA<sup>1</sup>. The intersection layout and reconstructed traffic are shown in Fig. 1. The comparison of our work and some example studies of intersections is illustrated in Fig. 2. To the best of our knowledge, our work is *the first to control and coordinate hybrid traffic at unsignalized intersections with both complicated topology and real-world traffic demands*.



Figure 1: Our study subjects include four complex intersections at Colorado Springs, CO, USA. The traffic is reconstructed using the actual traffic data collected at these intersections.

The control and coordination of intersection traffic pose many challenges, which include varied topology of intersections, changing traffic demands, and conflicting traffic streams. We propose a decentralized RL approach to handle these challenges. Our approach’s pipeline is shown in Fig. 3. First, after entering the control zone, each RV is controlled using our method

<sup>1</sup><https://coloradosprings.gov/>



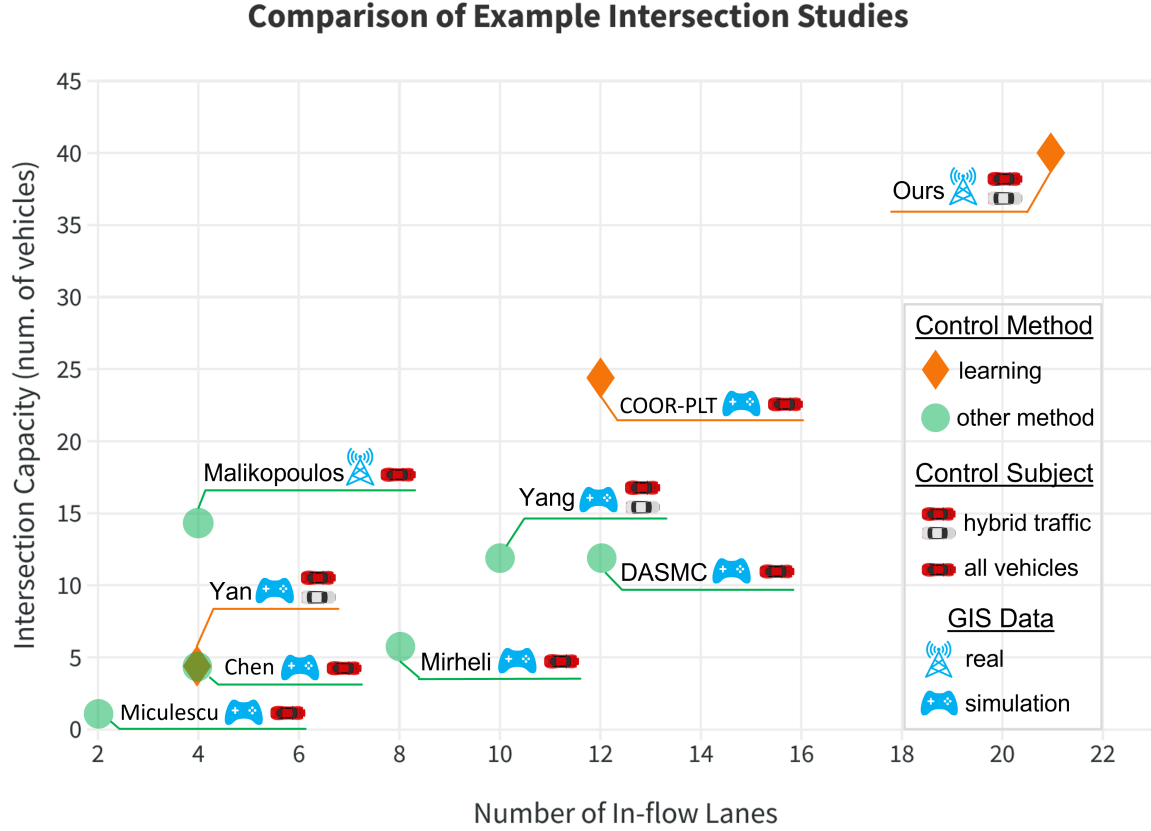


Figure 2: Comparison of some state-of-the-art studies on intersection traffic control. Ours and Yan are the only two studies applying RL to hybrid traffic control at intersections; between the two, ours is the only method based on real GIS data. Note that since not all measurements are provided, the shown features of each study are our best estimates after examining the study. For complete information, we refer readers to COOR-PLT (27), DASM (28), Yang (9), Malikopoulos (20), Mirheli (29), Chen (30), Yan (13), and Miculescu (19).

and is assumed to obtain a full observation of the traffic condition within the control zone. Next, each RV encodes the perceived traffic condition into a fixed-length representation. This representation contains traffic information of eight moving directions (see Fig. 3a). For each direction, both macroscopic traffic features such as queue length and waiting time, and microscopic traffic features such as vehicles’ locations inside the intersection are recorded. The representation is then adopted by each RV in front of the intersection entrance line to make a high-level decision ‘Stop’ or ‘Go’ (see Fig. 3b). The high-level decisions from different RVs in front of the entrance line are shared and coordinated via vehicle-to-vehicle (V2V) communication (Fig. 3c). Lastly, each RV travels through the intersection by fulfilling its high-level decision using a low-level control mechanism described in Sec. 4.5.2.

We conduct various experiments to evaluate our approach using the reconstructed traffic from real-world traffic data in SUMO (31). Our results show that with 50% or more RVs, our method outperforms traffic light control in terms of efficiency. In general, better performance is gained as the RV penetration rate increases from 50% to 100%. For example, the average waiting time is reduced by 16.08%, 40.29%, and 45.01% compared to traffic light control at the intersection 229 when the RV penetration rate is 50%, 70%, and 90%, respectively. With 100% RVs, our method can reduce the average waiting time of the entire intersection traffic up to 75% compared to traffic light control and 96% compared to the traffic light absence baseline. These results demonstrate the effectiveness of our approach. In addition, we analyze the reward function by Yan and Wu (13) and justify the design rationale of our reward function. We show that our local reward alternates between conflicting moving directions and grants a direction with a long-waiting queue the priority to travel. We also show that our global reward reflects the traffic condition of the entire intersection in a timely fashion. Then, we explore the relationship between traffic demands, congestion, and RV penetration rates. The results show that with just 5% RVs, we can prevent congestion at the intersection under the actual traffic demand of 700

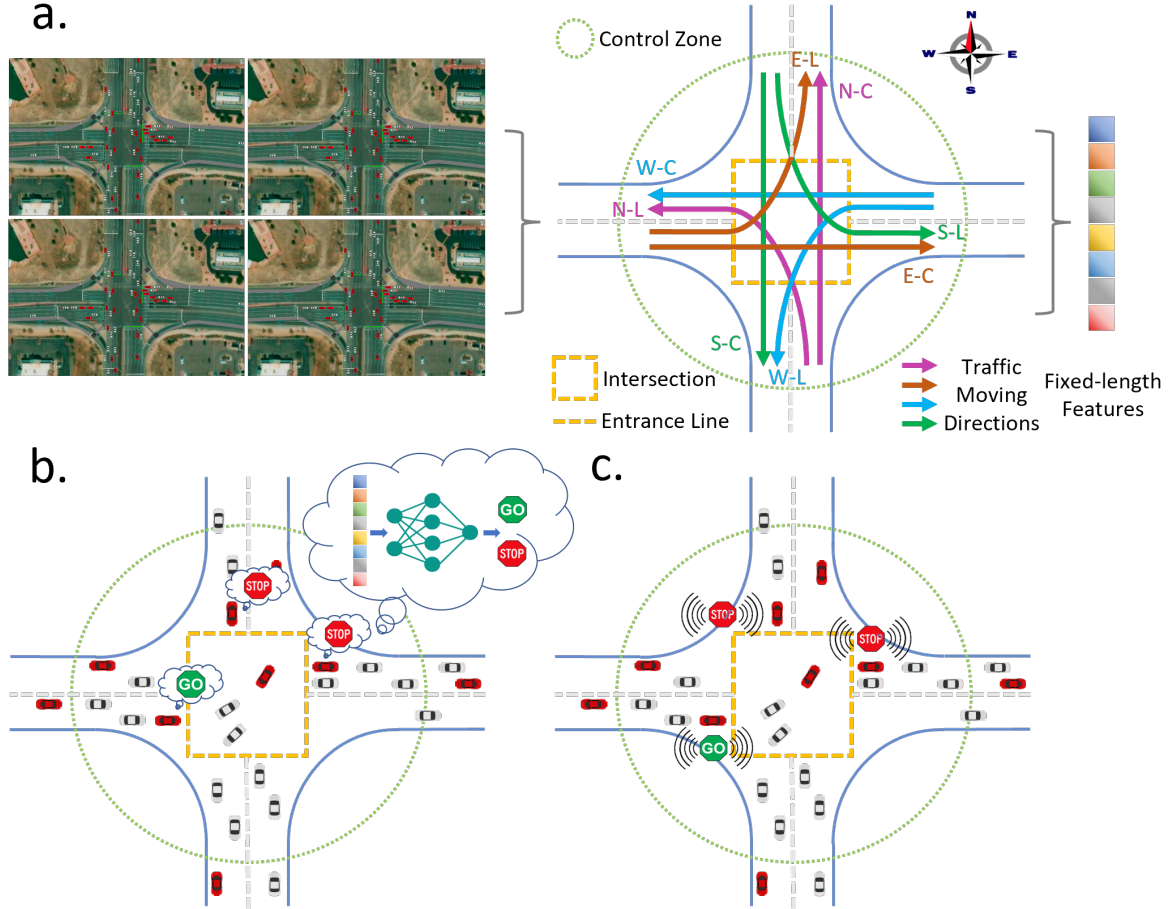


Figure 3: The pipeline of our approach. **a.** The traffic condition of an intersection is encoded by each RV inside the control zone to be a fixed-length representation. This representation contains both macroscopic traffic features such as queue length and waiting time, and microscopic traffic features such as vehicles' locations along each traffic moving direction (E, W, N, and S represent east, west, north, and south, respectively; C means cross and L means left-turn). **b.** The traffic-condition representation is then used by each RV in front of the entrance line to decide either 'Stop' or 'Go' at the high level. **c.** These high-level decisions of the RVs are communicated and coordinated to ensure conflict-free movements inside the intersection.

v/h. In contrast, without RVs, congestion emerges when the traffic demand is higher than 200 v/h. Lastly, we test the robustness and generalizability of our approach. For robustness, first we conduct a ‘blackout’ experiment when traffic lights suddenly stop working. During such an event, the RVs act as self-organized movable ‘traffic lights’ to coordinate the traffic and prevent congestion. Second, we examine the impact of sudden RV rate drops. The results demonstrate that even with 60% drop (from 100% to 40%), our method can still maintain stable and efficient traffic flows at the intersection. For generalizability, we deploy our method (without refining) in two unseen intersections: not only does our method prevent congestion, but starting from 50%–60% RVs, our method surpasses traffic light control on saving the average waiting time of all vehicles at the two intersections. The details of these results are introduced next.

## 2 Results

In this section, we first introduce the baselines for evaluating our method. Then, we present the overall results of our evaluations at four real-world intersections. Next, we present a series of experiments to analyze our reward function and discuss the insights of its design. After that, we explore the relationship between traffic demands, congestion, and RV penetration rates. Lastly, we demonstrate the robustness and generalizability of our approach to blackout events and unseen intersections, respectively.

### 2.1 Baselines

To evaluate our method, we compare our method with the following four baselines.

- **TL**: the actual traffic signal program deployed in the city of Colorado Spring, CO, USA.
- **NoTL**: no traffic light control; all traffic signals are off.
- **Yan (13)**: the state-of-the-art multi-agent RL traffic controller with 100% RV penetrate

rate. In order to use this approach, we make necessary changes to the approach to accommodate the varied intersection topology by extending the network input to the maximum number of incoming lanes in our work.

- **Yang (9)**: the state-of-the-art CAV control method for hybrid traffic at unsignalized intersections.

## 2.2 Overall Performance

We evaluate our approach under the RV penetration rates ranging from 40% to 100%. At each rate, we conduct ten experiments and report the averaged results. In each experiment, HVs are constructed using real-world traffic turning count data (see Sec. 4.2 for details). However, the behavior and location of each HV are stochastic. Each experiment runs for 1000 steps (1 step = 1 second in simulation). We use all four intersections shown in Fig. 1 for our experiments. The features of these intersections are given in Tab. S1.

The overall results measured using reduced average waiting time in percentage are listed in Table 1. The waiting time of a vehicle is the time that a vehicle spends in front of the entrance line waiting to enter the intersection. The average waiting time of a moving direction is then the average of the waiting times of all vehicles along that direction. The average waiting of an intersection is the average of the waiting times of all vehicles at the intersection. Overall, when the RV penetration rate is 50% or higher, our method outperforms traffic signals. Additionally, better performance is gained, in general, as the RV penetration rate increases. This shows that the more RVs can interact with their nearby HVs, the more stable the regulation and coordination of the entire traffic can be.

In Fig. 4, we show the detailed performance at intersection 229. The results include two parts. The first part (the top row of the four figures) shows the average waiting time along the eight traffic moving directions. Note that in the actual traffic data, some directions do not

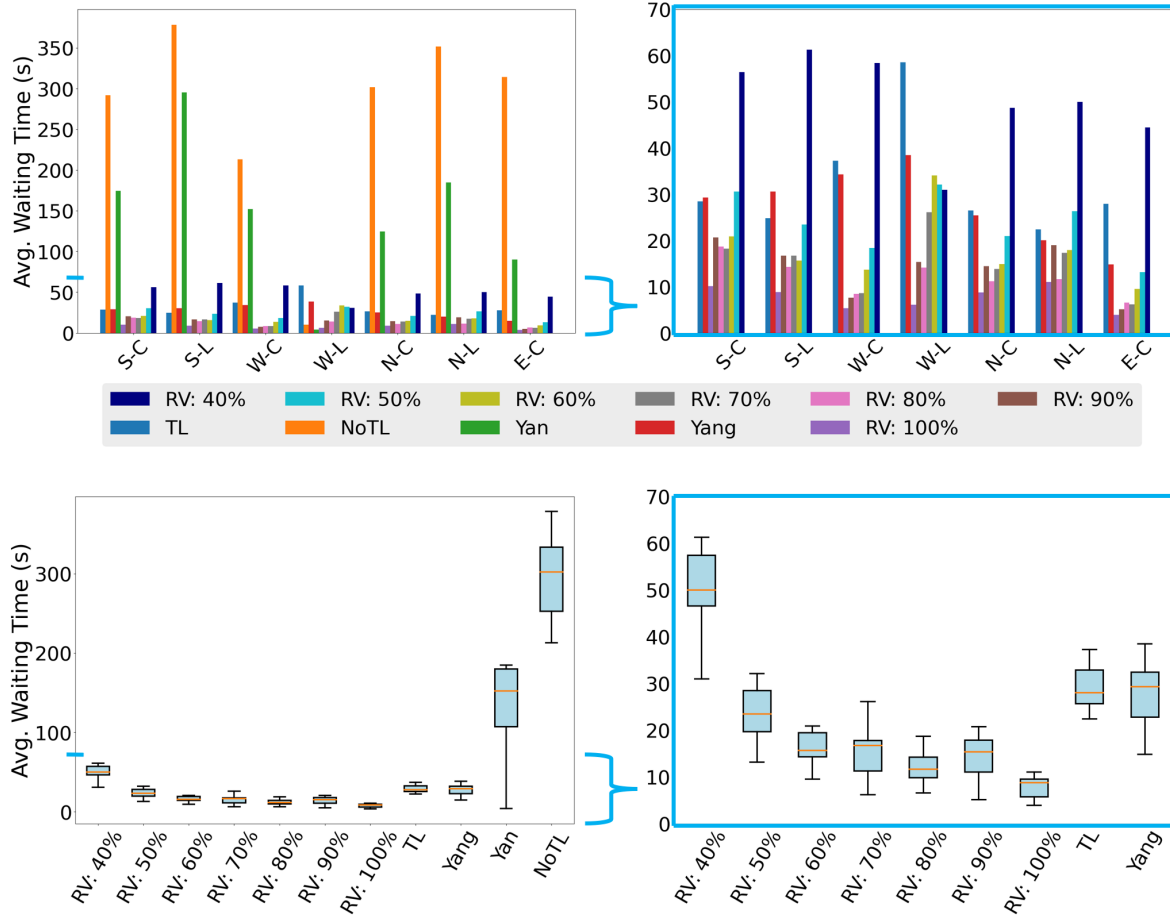


Figure 4: The overall results measured in average waiting time at the intersection 229. The RIGHT sub-figures are zoomed-in versions of the LEFT sub-figures by excluding NoTL and Yan. In general, as the RV penetration rate equals or passes 50%, our method achieves consistent better performance over the other four baselines.

Intersection	TL vs. RVs (%)						NoTL vs. RVs (%)
	50%	60%	70%	80%	90%	100%	100%
229	16.08%	44.02%	40.29%	58.35%	45.01%	68.62%	97.09%
449	22.67%	15.21%	32.56%	40.47%	43.06%	39.71%	75.03%
332	8.50%	1.20%	35.22%	31.86%	52.34%	61.15%	78.80%
334	57.42%	41.88%	59.51%	61.72%	64.67%	69.71%	64.43%

Table 1: Reduced average waiting time (in percentage) at each intersection under various RV penetration rates. When the RV penetration rate is 50% or higher, our method outperforms traffic signals across the board. In general, more time is saved as the RV penetration rate increases.

have traffic (e.g., E-L for 229) and thus are excluded from the results. The second part (the bottom row of the four figures) reports the influence of different RV penetration rates on the average waiting time. In the same way, Fig. S2, S3, and S4 illustrate the detailed performance at intersections 449, 332, and 334, respectively.

**Intersection 229.** As shown in Fig. 4, for all moving directions, NoTL and Yan perform the worst and are excluded from the zoomed-in sub-figure on the top, RIGHT row. From the zoomed-in sub-figure, we can see that the average waiting time is significantly reduced when the RV penetration rate is increased from 40% to 50% (except for W-L). Another major reduction of the waiting time is observed when the RV penetration rate further increases to 60%. For S-C, S-L, W-L, N-C, and N-L, approximately 40% to 60% additional saving in waiting time is achieved when the RV penetration rate increases from 90% to 100%. TL and Yang have similar performance on most moving directions, except for W-L and E-C where TL performs much worse than Yang. In general, our method starts to outperform TL and Yang when the RV penetration rate is 50% or higher.

We further show traffic congestion levels of intersection 229 during our evaluation in Fig. 5. The congestion level is defined as  $AVT/Threshold$ , where AVT denotes the average waiting time of all vehicles of a moving direction, and Threshold is for normalization. For results shown in Fig. 5, Threshold is set to 40, which is the maximum average waiting time during our evaluation



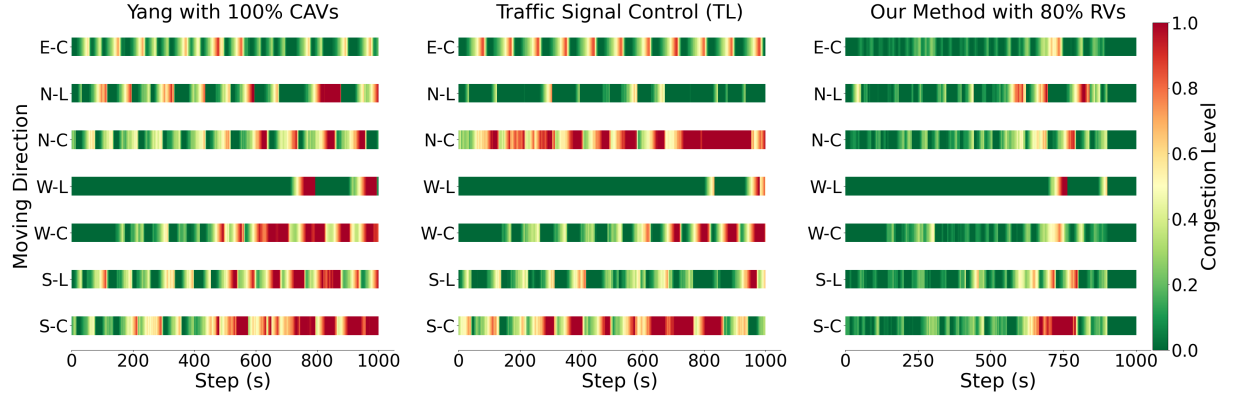


Figure 5: Traffic congestion levels at intersection 229 under different control mechanisms. Our approach with 80% RVs consistently achieves lower levels of congestion than Yang and TL. Unlike Yang and TL, which control intersection traffic using fixed phases, our method learns to use adaptive phases for control based on traffic conditions.

at intersection 229. The results illustrate that traffic controlled using our method achieves much lower congestion levels than Yang and TL. In addition, our method can flexibly coordinate conflicting moving directions based on varied traffic conditions, which is different than Yang and TL that employ fixed-phase coordination. These results hint that varied phases of control can positively influence the efficiency of intersection traffic.

**Intersection 449.** In general, similar results are observed as those of intersection 229 and are shown in Fig. S2. For most moving directions, the performances of Yan and NoTL are worse than ours, except for the direction W-L. Our method with 50% RVs or higher outperforms Yang and TL in nearly all cases.

**Intersection 332.** The results are shown in Fig. S3. We can see that the average waiting time decreases as the RV penetration rate increases from 40% to 100%. Similar to the intersections 229 and 449, Yan and NoTL are worse than Yang and TL, as well as our method with RV penetration rate 40% or higher, except for the S-C direction. For Yang and TL, our method with at least 70% RVs can outperform them at all moving directions.

**Intersection 334.** The results are shown in Fig. S4. In general, the average waiting time

decreases as the RV penetration rate increases. There is an interesting phenomenon where the median of the average waiting time of NoTL is lower than that of TL. This is because intersection 334 has a lower traffic demand than the other three intersections. The peak flow is 515 vehicles per lane per hour compared to around 700 for the other three intersections. This lowers the chance of congestion inside the intersection and makes the absence of traffic lights less an obstacle for efficient traffic flows.

Worth mentioning, across all results of all intersections, the average waiting time of all vehicles may not monotonically decrease when the RV penetration rate increases. The median waiting time of a higher RV percentage can be lower than the median waiting time of a lower RV percentage, e.g., 60% RVs vs 50% RVs at the intersection 449. This is because during repeated experiments, while traffic demands are matched between simulations, the actual data, behaviors, and positions of individual vehicles are stochastic. These unpredictable factors can lead to a large variance in performance.

### **2.3 Hybrid Reward**

Reward design is essential to RL. A poorly designed reward can result in inferior performance of a control task; however, it is non-trivial to design a reward for complex tasks that reflects all desiderata of a task and benefits from the convergence of the learning process. Our task is intrinsically complex: varied topology and conflicting traffic streams can lead to conflicts inside the intersection, and the use of real-world traffic data can lead to unpredictable and unstable inflow/outflow for the road network.

To resolve conflicting movements within the intersection and avoid the negative impact of traffic jams on the learning process, we design our reward function by fusing the collision punishment and the conflict punishment to prevent intersection conflicts. Our insight is to design the reward function into two parts: a local reward and a global reward. The local reward quan-

tifies the influence of each RV’s actions on the waiting time and queue length of the traffic on its own moving direction while the global reward concerns the performance of the whole intersection and encourages RVs from conflicting directions to cooperate (32). According to our experiments, our hybrid reward enables effective and efficient interchange of traffic streams at the intersection. More details of our hybrid reward is presented in Sec. 4.4.3.

To illustrate why our reward function works for large-scale traffic scenarios, we show an example global reward in the logarithmic scale at the bottom, LEFT row of Fig. S1. As shown by the results, our global reward responds to the change of traffic conditions swiftly and thus is a timely indicator for the learning process. The global reward is defined in Sec. 4.4.3. When congestion eases, it will be positive; on the other hand, it will be negative if congestion worsens. Regarding the local reward, we show that it alternates between conflicting moving directions in the MIDDLE and RIGHT sub-figures of Fig. S1. Since the local reward focuses on the traffic condition on each RV’s own moving direction, the RV is encouraged to release a long-waiting queue to cross the intersection. Again, the local reward is detailed in Sec. 4.4.3.

We also analyze the limitation of the state-of-the-art method’s reward function in Text S1, which furthers the design rationale of our reward function.

## 2.4 Traffic Demands, Congestion, and RV Percentages

In previous sections, we show that under real-world traffic demands with traffic signals off, congestion starts to develop along with the average waiting time of all vehicles increasing significantly. In this section, we use intersection 229 as the testbed to further explore the relationship of traffic demands and congestion. The results of our first set of experiments are shown in Fig. S5 LEFT. By increasing the traffic demand from 150 v/h to 300 v/h under no traffic lights and no RVs, we can see that starting from 200 v/h, congestion starts to form (reflected by the low average speed of all vehicles at the intersection). For comparison, we show the actual

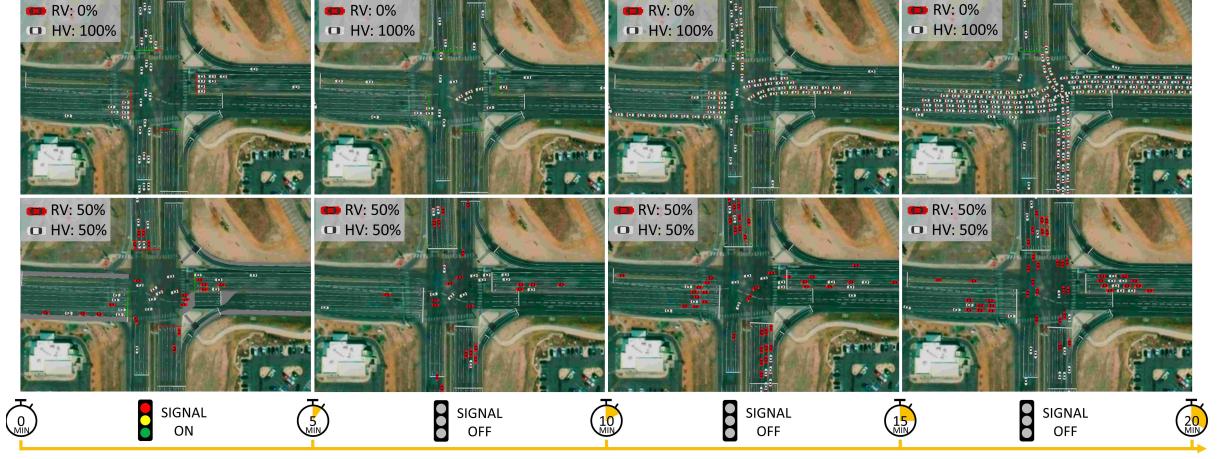


Figure 6: Comparison between traffic conditions with and without RVs during a blackout event at the intersection 229. The blackout event occurs at the 5-minute mark, when all traffic signals stop working. For traffic without RVs, congestion quickly forms within the next 15 minutes. In contrast, for traffic with RVs controlled using our approach, no congestion is observed.

traffic demand at intersection 229 of  $\sim 700$  v/h. Although the real-world demand is significantly higher than the 200 v/h demand that causes congestion, no congestion forms with just 5% RVs deployed in traffic. Fig. S5 RIGHT additionally shows that the minimal RV penetration rate needed to prevent congestion under the real-world traffic demand at the intersection is 5%.

## 2.5 Robustness

To demonstrate the robustness of our approach, we simulate several blackout events, during which all traffic signals are off. The results comparing no RVs and 50% RVs are shown in Fig. 6. In Fig. S6, the blackout event occurs at the 100th step. We can observe that if there exists no RVs, the average waiting time increases significantly due to traffic jams when traffic lights are absent. Once the traffic lights are turned off, the intersection is fully congested. In contrast, with 50% RVs, the average waiting time remains stable during the blackout event. In essence, RVs controlled using our method perform like ‘self-organized traffic lights’ to coordinate the traffic at the intersection and prevent gridlocks.

In Fig. S7, we show the impact of sudden RV percentage drops on the intersection traffic. These sudden drops can be caused by unstable V2V communication, other unforeseeable software failures, or humans taking over the control. The ‘offline’ RVs are taken over by Intelligent Driver Model (IDM) (33), which is used for all HVs. All drops occur at the 100th step. As expected, the average waiting time of all vehicles at the intersection increases. Nevertheless, our method can successfully and quickly stabilize the system and contain the average waiting time under certain thresholds.

## 2.6 Generalization

To evaluate the generalizability of our approach, we test on two unseen intersections. These two intersections are also taken from the city of Colorado Springs and are shown in Fig. S8. Notice that one test scenario is a three-legged intersection, which has a different topology than all our training intersections (which are all four-legged). The detailed parameters of the intersections are shown in Tab. S2.

For the unseen four-legged intersection, we directly deploy our trained model without refining it. The result is illustrated in Fig. S9. Our method works well and beats the traffic light control baseline when the RV penetration rate is 60% or higher. With 100% RVs, our method can reduce the average waiting time by almost 80% compared to the traffic light control baseline.

We also deploy our trained model without refining it on the unseen three-legged intersection. Since it is a three-legged intersection, there are only four directions that need to be coordinated, namely S-C, S-L, W-L, and N-C. We set the corresponding input values of other directions (appearing in four-legged intersections) to zero for our RL policy. The result is shown in Fig. S10. The intersection is jammed when the traffic lights are absent. The average waiting time of the NoTL baseline is much higher than others. Although our RL model has never seen this inter-

section and the traffic demand, it still manages to coordinate the traffic and prevent congestion at the intersection. Our approach outperforms the traffic light control baseline when the RV penetration rate is 50% or higher. Our method with 100% RVs can reduce the average waiting time by  $\sim 30\%$  compared to the traffic light control baseline. These results demonstrate the excellent generalizability of our approach.

### 3 Conclusion

We propose a decentralized RL approach for the control and coordination of hybrid traffic at real-world and unsignalized intersections. Our approach consists of three novel techniques to handle the complexities of intersections: 1) an encoder to convert the traffic status into a fixed-length representation, 2) a hybrid reward function that suits large-scale intersectional traffic, and 3) a coordination mechanism to ensure conflict-free movements. Our method is the first to control hybrid traffic under real-world traffic conditions at complex intersections. Various experiments are conducted to show the effectiveness, robustness, and generalizability of our approach. Detailed analysis are also pursued to justify the design choices of the components of our method.

In the future, we would like to further improve our method in three aspects. First, the learning algorithm could use a hierarchical design so that the low-level control (e.g., longitudinal and lateral acceleration) also becomes the RL policy’s output. Second, we want to ease the coordination mechanism so that vehicles have more freedom to move inside the intersection. Nevertheless, we anticipate that certain prior knowledge remains necessary for ensuring no-conflict movements. Finally, we would like to combine our approach with traffic flow prediction to further improve the performance of coordination: real-world traffic demands fluctuate over time, thus accurate flow predictions are very useful in enhancing the effectiveness of the control and coordination of intersection traffic.

## 4 Methodology

### 4.1 Intersection Topology and Conflicting Traffic Streams

For a common four-legged intersection, there are four moving directions: eastbound (E), westbound (W), northbound (N), and southbound (S); and three turning options at the intersection: left (L), right (R), and cross (C). As an example, we use E-L and E-C to denote left-turning traffic and crossing traffic that travel eastbound before entering the intersection, respectively. The complete notation is shown in Fig. 3a. Inside the intersection, conflicts may occur among the moving directions. Here, we define ‘conflict’ as two moving directions intersecting each other, e.g., E-C and N-C. It is worth noting since the right-turning traffic will not enter the intersection (or will only occupy the intersection for a short period of time), we do not coordinate right-turning traffic with traffic from other directions. Our experiments show that this empirical choice has minimal effects on the control and coordination of intersection traffic.

In summary, we consider eight traffic streams that can potentially raise conflicts: E-L, E-C, W-L, W-C, N-L, N-C, S-L, and S-C. We further define the conflict-free movement set  $\mathcal{C} = \{(S-C, N-C), (W-C, E-C), (S-L, N-L), (E-L, W-L), (S-C, S-L), (E-C, E-L), (N-C, N-L), (W-C, W-L)\}$ . For each pair in  $\mathcal{C}$ , the two traffic streams will not conflict with each other; however, conflicts can potentially occur in the remaining traffic stream pairs.

### 4.2 Traffic Reconstruction and Simulation

In order for robot vehicles to interact with human-driven vehicles under real-world traffic conditions, we need to first reconstruct traffic using actual traffic data and then carry on high-fidelity simulations. We reconstruct the intersection traffic using turning count data at each intersection provided by the city of Colorado Springs, CO, USA<sup>2</sup>. The turning count data records the number of vehicles moving in a particular direction at the intersection and is collected via in-road

---

<sup>2</sup><https://coloradosprings.gov/>



sensors such as infrastructure-mounted radars.

Given the GIS data (traffic data and digital map), we pursue traffic simulations in SUMO (31), a widely-adopted high-fidelity traffic simulation platform. The reconstructed traffic and traffic simulations are showcased in Fig. 1. In SUMO, a directed graph is used to describe the simulation area. Each edge of the graph represents a road segment with an ID and a vehicle’s route is defined by a list of edge IDs. Vehicles are then routed using jtrouter<sup>3</sup> in SUMO based on the turning count data. By default, jtrouter will select edges that are close to the intersection as the starting and ending edges of a route. This type of route can be extremely short and affect the simulation fidelity. To mitigate this issue, we adjust the vehicle routes by proposing more proper edges for the vehicles to enter and leave the network. Specifically, for the traffic stream on the main road that connects the four intersections, we assign the starting and ending edges of the routes to the boundary of the main road; for the traffic stream on other roads, the starting edges are moved to the successor upstream intersection and the ending edges are moved to the successor downstream intersection. After re-assigning the starting edge and ending edge of each route, ‘extra traffic counts’ can occur. For example, a vehicle traveling through intersection 334 from northbound can also travel through intersections 229, 449, and 332, contributing to the northbound count for all four intersections. To alleviate this problem, we consider the coordination of traffic flows among adjacent intersections to avoid traffic double-counting, and then refine the number of routes to ensure the turning counts in the simulation match the actual turning count data. Fig. 1 shows the four intersections in our study. To evaluate whether the simulated flow resembles the real-world flow in terms of turning counts, we adopt the absolute percentage error (APE):

$$APE = \frac{|TC_{\text{real}} - TC_{\text{sim}}|}{TC_{\text{real}}}, \quad (1)$$

where  $TC_{\text{real}}$  and  $TC_{\text{sim}}$  are the turning counts from the real-world traffic and simulated traffic,

---

<sup>3</sup><https://sumo.dlr.de/docs/jtrrouter.html>

respectively. As a result, the APE score for intersections 229, 499, 332, and 334 are 0.22, 0.21, 0.16, and 0.17, respectively. Since  $\text{APE} = 0$  means the exact match of simulated and real-world traffic, these low APE scores (i.e.,  $\sim 0.2$ ) verify the fidelity of our simulations.

### 4.3 Hybrid Traffic Generation

To create a mixture of robot and human-driven vehicles, at each time step, newly spawned vehicles are randomly assigned to be either a robot vehicle (RV) or a human-driven vehicle (HV) according to a pre-specified RV penetration rate. For an HV, the longitudinal acceleration is computed using Intelligent Driver Model (IDM) (33). For an RV, when it is outside the control zone, IDM is again used to determine the longitudinal acceleration; if it is inside the control zone, the high-level decisions ‘Stop’ and ‘Go’ are determined by the RL policy, while its low-level longitudinal acceleration is determined by the control method described in Sec. 4.5.2.

### 4.4 Decentralized RL For Hybrid Traffic

We formulate the control of RVs at the interaction as a POMDP, which consists of a 7-tuple  $(\mathcal{S}, \mathcal{A}, \mathcal{T}, \mathcal{R}, \Omega, \mathcal{O}, \gamma)$ , where  $\mathcal{S}$  is a set of states ( $\mathbf{s} \in \mathcal{S}$ ),  $\mathcal{A}$  is a set of actions ( $\mathbf{a} \in \mathcal{A}$ ),  $\mathcal{T}$  is the transition probabilities between states  $\mathcal{T}(\mathbf{s}' | \mathbf{s}, \mathbf{a})$ ,  $\mathcal{R}$  is the reward function ( $\mathcal{S} \times \mathcal{A} \rightarrow \mathbb{R}$ ),  $\Omega$  is a set of observations  $\mathbf{o} \in \Omega$ ,  $\mathcal{O}$  is the set of conditional observation probabilities and  $\gamma \in [0, 1)$  is a discount factor. In our task, at each time  $t$ , when an RV  $i$  enters the control zone of an intersection, its action  $a_i^t$  is determined based on its observation (of the current traffic condition)  $o_i^t$ , which is a partial observation of the traffic state  $s_i^t$  at the intersection. Such a problem can be solved using RL (34), where the policy  $\pi_\theta$  is a neural network trained using the following loss:

$$L = \left( R_{t+1} + \gamma_{t+1} q_{\bar{\theta}} \left( S_{t+1}, \arg \max_{a'} q_\theta(S_{t+1}, a) \right) - q_\theta(S_t, A_t) \right)^2. \quad (2)$$

In Eq. 2,  $q$  denotes the estimated value from the value network,  $\theta$  and  $\bar{\theta}$  respectively represent the value network and the target network. The target network is a periodic copy of the value

network, which is not directly optimized during training. Next, we detail the components (i.e., action space, observation space, reward function) as well as the whole pipeline of our decentralized RL algorithm.

#### 4.4.1 Action Space

Since our focus is to control hybrid traffic via the influence of RVs to HVs in a more advantageous way than traffic lights, we design the action space of RVs to only consist of high-level decisions. To be specific, an RV’s action  $a_i^t$  determines at time  $t$  whether the RV  $i$  shall pass the entrance line of an intersection or stop at the entrance line to block its following vehicles:

$$a_i^t \in A = \{\text{Stop}, \text{Go}\}. \quad (3)$$

When the RL policy grants ‘Go’, the RV will enter the intersection; instead, if the RL policy decides ‘Stop’, the RV will decelerate and stop at the entrance line.

#### 4.4.2 Observation Space

In order to develop a general RL policy that can handle varied intersection topology and the number of connecting lanes, we encode the traffic conditions observed by each RV to a fixed-length representation. Specifically, the observation of each RV in the control zone (starts at 30m before the entrance line) includes three elements:

- The status of the RV. The status includes one feature—the distance, denoted as  $d_i^t$ , between the RV  $i$ ’s position to the entrance line of the intersection.
- Traffic condition outside the intersection (but inside the control zone). As introduced in Sec. 4.1, we categorize traffic streams into eight movement groups. We compute the queue length  $l^{t,j}$  and the average waiting time  $w^{t,j}$  of each group  $j$  at time  $t$ . This is

to quantify the anisotropic congestion levels at an intersection. These features can be conveniently shared among all vehicles in the control zone via local communication.

- Traffic condition inside the intersection. We design an ‘occupancy map’  $m^{t,j}$  for each moving direction  $j$  inside the intersection. As shown in Fig. S11, for each direction, an inner lane is divided into 10 equal segments. If a vehicle’s position falls into a segment, that segment is considered occupied and its value is set to 1. An empty segment’s value is set to 0.

Overall, the observation of RV  $i$  at time  $t$  is defined as:

$$o_i^t = \oplus_j^J \langle l^{t,j}, w^{t,j} \rangle \oplus_j^J \langle m^{t,j} \rangle \oplus \langle d_i^t \rangle, \quad (4)$$

where  $\oplus$  is the concatenation operator and  $J = 8$  is the number of traffic moving directions at the intersection.

#### 4.4.3 Hybrid Reward

To encourage the RV not only consider its own efficiency but also the efficiency of the entire intersection traffic, we design a hybrid reward function for the RV taking the following form:

$$r(s^t, a^t, s^{t+1}) = \lambda_L r_L + \lambda_G r_G, \quad (5)$$

where  $r_L$  is the local reward,  $r_G$  is the global reward, and  $\lambda_L$  and  $\lambda_G$  are the coefficients of the two rewards, respectively.

The local reward  $r_L$  is defined as

$$r_L = \begin{cases} 0 & \text{if } a^t = \text{Stop} \\ -100 & \text{else if conflict occurs} \\ (OF^j(s^t, s^{t+1}) + QL^j(s^{t+1})) \cdot AW^j(s^{t+1}) & \text{otherwise} \end{cases} \quad (6)$$

where  $OF^j(s^t, s^{t+1})$  denotes the outflow, i.e., the number of vehicles entering the intersection, along the movement direction  $j$  during the time period  $[t, t + 1]$ .  $QL^j(s^{t+1})$  is queue length of

the traffic waiting at the  $j$ th moving direction to enter the intersection.  $AW^j(s^t)$  is the average waiting time of all vehicles in the corresponding  $j$ th queue at time step  $t$ . If the current action is ‘Stop’, the local reward is 0. If the current action is ‘Go’, but the RV’s movement conflicts with other vehicles passing through the intersection, it will be punished with  $-100$ . On the other hand, if the RV’s ‘Go’ action does not conflict with other vehicles, it will get a positive reward value because  $OF^j(s^t, s^{t+1})$ ,  $QL^j(s^{t+1})$ , and  $AW^j(s^t)$  are non-negative.

The global reward  $r_G$  is defined as

$$r_G = \sum_j^J (QL^j(s^t) \cdot AW^j(s^t)) - \sum_j^J (QL^j(s^{t+1}) \cdot AW^j(s^{t+1})), \quad (7)$$

where the left side of the minus sign is the summation of the average waiting time multiplied by the queue length of each direction  $j$  at  $t$ , which measures the severity of traffic congestion; the right side of the minus sign measures the severity of traffic congestion at  $t + 1$ . Hence, the global reward reveals the change in traffic congestion during one time step. The design of Eq. 7 is inspired by the observation that both waiting time and queue length (35, 36) have been adopted to quantify traffic congestion. However, we find that either metric alone is less informative to quantify the congestion level formed by hybrid traffic at complex intersections. While there are infinitely many ways to combine both metrics to form the reward, we choose a non-linear approach, i.e., multiplying them together, over other linear options. This is because hybrid traffic represents an unstable and non-preemptive system. The relationship between waiting time and queue length does not obey the Little’s law (37) and thus does not take a linear form. Extensive experiments show that our hybrid reward enables effective interchanges of traffic streams at the intersection. The analysis of the hybrid reward is elaborated in Sec. 2.3.

#### 4.4.4 RL Algorithm

For the actual RL algorithm, we adopt Rainbow DQN (34). Rainbow DQN is a state-of-the-art technique that combines the novel designs of six extensions of the original DQN algorithm (38),

including prioritized experience replay (39), double DQN (40), dueling network (41), distributional RL algorithm (42), and noisy network (43). By incorporating the advantages of these DQN variants, Rainbow DQN achieves the best performance on the Atari benchmark (34). We use Rainbow DQN and the hybrid reward function to centrally train all RVs. During execution, each RV executes its own policy and all RVs share the same policy, i.e., the same neural network architecture and weights.

To be specific, the policy  $\pi_\theta$  is represented by a neural network with three fully connected (FC) layers. Each FC layer contains 512 hidden units and uses a rectified linear unit (ReLU) as the activation layer. For training, the learning rate is set to  $1e-3$ , the discount factor is set to 0.99, and the batch size of each policy update is 2048. We train our model using a PC with Intel i9-9900K and NVIDIA GeForce RTX 2080Ti. The training time varies due to different RV penetration rates, but in general 48 hours are expected for a policy to converge.

## 4.5 Traffic Coordination and Low-level Control

### 4.5.1 Resolving Conflicting Traffic Streams

Conflicted movements are the most crucial aspects of intersection traffic, which can cause gridlocks not only locally at each intersection but potentially over the entire traffic network (9). Although our approach punishes conflicting movements (through the hybrid reward function), learning-based autonomous systems that are simultaneously effective and provably safe remain an open problem (44). So, conflicts can still occur and subsequently affect the training efficiency. To ensure our approach is conflict-free, we introduce a coordination mechanism to post-process the decisions returned by the RL policy. This mechanism is applied only to the traffic stream pairs that are not defined in the non-conflict movement set  $\mathcal{C}$ .

First, each RV obtains its ‘Stop’ or ‘Go’ decision by the RL policy. Then, the RV broadcasts its decision among all RVs inside the control zone. Next, each RV (ego RV) at the entrance line

compares its decision with all other RVs in the control zone. This comparison results in three conditions:

- If the vehicles inside the intersection are on the conflicting stream of ego RV, the ego RV is not permitted to enter the intersection.
- If the vehicles inside the intersection are not on the conflicting stream of the ego RV, but multiple RVs at the entrance line on conflicting streams receive the decision ‘Go’ in the same time step (a potential conflict decision), a priority score is calculated as the product of average waiting time and queue length. The RV with the highest score can enter the intersection, while other RVs should wait at the entrance line.
- If the vehicles inside the intersection are not on the conflicting stream of the ego RV and there are no potential conflict decisions for the ego RV, the ego RV will execute its decision.

Since the hybrid reward function contains a punishment term for conflict decisions, the agent will learn to avoid conflicts during training. In Fig. S12 LEFT, we show that the number of conflict decisions decreases as the training progresses, and the trend stabilizes at a low level after the corresponding policy converges. We also investigate the conflict rate computed as the number of conflict decisions divided by the number of RVs inside the control zone. As shown in Fig. S12 RIGHT, the conflict rate of either 60% RVs or 80% RVs tends to converge around 5%, while the conflict rate of 100% RVs approaches 0 after 500 steps. The results demonstrate the effectiveness of the RL policy in coordinating intersection traffic and the infrequent use cases of the coordination mechanism introduced in this section.

#### **4.5.2 Low-level Control of RVs**

While the RL policy makes the high-level decisions ‘Stop’ and ‘Go’, low-level controls are needed to complement an RV for traveling through the intersection.



- Route planning. The route of a vehicle is planned during the traffic reconstruction phase (discussed in Sec. 4.2). There is no re-planning of a vehicle’s route during the simulation phase.
- Longitudinal acceleration. For RVs receiving the decision ‘Go’, their longitudinal acceleration will be set to the vehicle’s maximum acceleration  $a^t = a_{\max}$ ; for RVs receiving the decision ‘Stop’, they will slow down and stop at the entrance line using the deceleration  $a^t = \frac{-v^2}{2 \cdot d_{\text{front}}}$ , where  $d_{\text{front}}$  is the distance to the entrance line. Note that other deceleration computing methods can be adopted to replace our formula.

## 4.6 Assumptions of RVs

It is important to note that the RVs defined in this project are different than the conventional set-ups of autonomous vehicles (AVs), which are equipped with a complete suite of perception-to-planning modules. Our RVs focus on the high-level decisions of ‘Stop’ and ‘Go’ and only require a certain form of V2V communication to obtain vehicles’ positions inside the control zone. Other types of sensors such as cameras and lidars are unnecessary. Thus, our learning process is different than a typical training process (end-to-end or otherwise) of autonomous driving. Another important difference between our RV and the conventional AV is that our RV does not exclude humans but can keep humans in the loop: humans can execute the low-level controls of an RV while the machine learning module suggests the ‘Stop’ or ‘Go’ decisions. Monetary incentive mechanisms can be established to encourage humans to follow the suggestions and contribute to more efficient traffic systems. In case that the suggestions are not followed regularly, the hybrid traffic system can still benefit from the proposed control mechanism as the RV penetration rate steadily increases in the expected future (see Sec. 2.5). Overall, the above-mentioned characteristics make our RVs applicable to all levels of vehicle autonomy and a more practical solution for facilitating intersection traffic than using fully equipped AVs.

## References

1. David Schrank, Bill Eisele, Tim Lomax, and Jim Bak. Urban mobility scorecard. *Texas A&M Transportation Institute and INRIX*, 2021.
2. United Nations. World urbanization prospects: The 2018 revision (st/esa/ser.a/420). *Department of Economic and Social Affairs, Population Division, New York: United Nations*, 2019.
3. Mallory Trouve, Gaelle Lesteven, and Fabien Leurent. Worldwide investigation of private motorization dynamics at the metropolitan scale. *Transportation Research Procedia*, 48:3413–3430, 2020.
4. Eun-Ha Choi. Crash factors in intersection-related crashes: An on-scene perspective. *National Highway Traffic Safety Administration, U.S. Department of Transportation*, 2010.
5. Associated Press. Power still out to 50k customers, days after memphis storm. <https://www.usnews.com/news/best-states/tennessee/articles/2022-02-07/power-still-out-to-60k-customers-days-after-memphis-storm>, February 2022.
6. Ben Winck. Get ready for blackouts from london to la, as the global energy crisis overwhelms grids and sends energy prices skyrocketing. <https://www.businessinsider.com/global-europe-energy-crisis-power-electricity-outages-blackouts-energy-op=1>, September 2022.

7. Rachel Ramirez. Power outages are on the rise, led by texas, michigan and california. here's what's to blame. <https://www.cnn.com/2022/09/14/us/power-outages-rising-extreme-weather-climate/index.html>, September 2022.
8. Guni Sharon and Peter Stone. A protocol for mixed autonomous and human-operated vehicles at intersections. In *International Conference on Autonomous Agents and Multiagent Systems*, pages 151–167, 2017.
9. Hao Yang and Ken Oguchi. Intelligent vehicle control at signal-free intersection under mixed connected environment. *IET Intelligent Transport Systems*, 14(2):82–90, 2020.
10. Cathy Wu, Abdul Rahman Kreidieh, Kanaad Parvate, Eugene Vinitsky, and Alexandre M Bayen. Flow: A modular learning framework for mixed autonomy traffic. *IEEE Transactions on Robotics*, 38(2):1270–1286, 2022.
11. Eugene Vinitsky, Kanaad Parvate, Aboudy Kreidieh, Cathy Wu, and Alexandre Bayen. Lagrangian control through deep-rl: Applications to bottleneck decongestion. In *IEEE International Conference on Intelligent Transportation Systems*, pages 759–765, 2018.
12. Shuo Feng, Xintao Yan, Haowei Sun, Yiheng Feng, and Henry X Liu. Intelligent driving intelligence test for autonomous vehicles with naturalistic and adversarial environment. *Nature communications*, 12(1):1–14, 2021.
13. Zhongxia Yan and Cathy Wu. Reinforcement learning for mixed autonomy intersections. In *IEEE International Intelligent Transportation Systems Conference*, pages 2089–2094, 2021.
14. Kathy Jang, Eugene Vinitsky, Behdad Chalaki, Ben Remer, Logan Beaver, Andreas A Malikopoulos, and Alexandre Bayen. Simulation to scaled city: zero-shot policy transfer for

- traffic control via autonomous vehicles. In *ACM/IEEE International Conference on Cyber-Physical Systems*, pages 291–300, 2019.
15. Jackeline Rios-Torres and Andreas A Malikopoulos. A survey on the coordination of connected and automated vehicles at intersections and merging at highway on-ramps. *IEEE Transactions on Intelligent Transportation Systems*, 18(5):1066–1077, 2016.
  16. PB Hunt, DI Robertson, RD Bretherton, and RI Winton. Scoot-a traffic responsive method of coordinating signals. Technical report, Transport and Road Research Laboratory (TRRL), United Kingdom, 1981.
  17. Mohammed A Hadi and Charles E Wallace. Hybrid genetic algorithm to optimize signal phasing and timing. *Transportation Research Record*, (1421):104–112, 1993.
  18. Mohammed A Hadi and Charles E Wallace. Optimization of signal phasing and timing using cauchy simulated annealing. *Transportation Research Record*, 1456:64–71, 1994.
  19. David Miculescu and Sertac Karaman. Polling-systems-based autonomous vehicle coordination in traffic intersections with no traffic signals. *IEEE Transactions on Automatic Control*, 65(2):680–694, 2019.
  20. Andreas A Malikopoulos, Christos G Cassandras, and Yue J Zhang. A decentralized energy-optimal control framework for connected automated vehicles at signal-free intersections. *Automatica*, 93:244–256, 2018.
  21. Bowen Baker, Ingmar Kanitscheider, Todor Markov, Yi Wu, Glenn Powell, Bob McGrew, and Igor Mordatch. Emergent tool use from multi-agent autocurricula. In *International Conference on Learning Representations*, 2020.

22. Oriol Vinyals, Igor Babuschkin, Wojciech M Czarnecki, Michaël Mathieu, Andrew Dudzik, Junyoung Chung, David H Choi, Richard Powell, Timo Ewalds, Petko Georgiev, et al. Grandmaster level in starcraft ii using multi-agent reinforcement learning. *Nature*, 575(7782):350–354, 2019.
23. Christopher Berner, Greg Brockman, Brooke Chan, Vicki Cheung, Przemysław Dębiak, Christy Dennison, David Farhi, Quirin Fischer, Shariq Hashme, Chris Hesse, et al. Dota 2 with large scale deep reinforcement learning. *arXiv preprint arXiv:1912.06680*, 2019.
24. William H Guss, Brandon Houghton, Nicholay Topin, Phillip Wang, Cayden Codel, Manuela Veloso, and Ruslan Salakhutdinov. Minerl: A large-scale dataset of minecraft demonstrations. In *International Joint Conference on Artificial Intelligence*, pages 2442–2448, 2019.
25. Maximilian Jaritz, Raoul De Charette, Marin Toromanoff, Etienne Perot, and Fawzi Nashashibi. End-to-end race driving with deep reinforcement learning. In *IEEE International Conference on Robotics and Automation*, pages 2070–2075, 2018.
26. Zhongxia Yan, Abdul Rahman Kreidieh, Eugene Vinitsky, Alexandre M Bayen, and Cathy Wu. Unified automatic control of vehicular systems with reinforcement learning. *IEEE Transactions on Automation Science and Engineering*, 2022.
27. Duowei Li, Jianping Wu, Feng Zhu, Tianyi Chen, and Yiik Diew Wong. Coor-plt: A hierarchical control model for coordinating adaptive platoons of connected and autonomous vehicles at signal-free intersections based on deep reinforcement learning. *arXiv preprint arXiv:2207.07195*, 2022.

28. Anye Zhou, Srinivas Peeta, Menglin Yang, and Jian Wang. Cooperative signal-free intersection control using virtual platooning and traffic flow regulation. *Transportation research part C: emerging technologies*, 138:103610, 2022.
29. Amir Mirheli, Mehrdad Tajalli, Leila Hajibabai, and Ali Hajbabaie. A consensus-based distributed trajectory control in a signal-free intersection. *Transportation research part C: emerging technologies*, 100:161–176, 2019.
30. Xiaolong Chen, Manjiang Hu, Biao Xu, Yougang Bian, and Hongmao Qin. Improved reservation-based method with controllable gap strategy for vehicle coordination at non-signalized intersections. *Physica A: Statistical Mechanics and its Applications*, page 127953, 2022.
31. Michael Behrisch, Laura Bieker, Jakob Erdmann, and Daniel Krajzewicz. SUMO—simulation of urban mobility: an overview. In *International Conference on Advances in System Simulation*, 2011.
32. Behrad Toghi, Rodolfo Valiente, Dorsa Sadigh, Ramtin Pedarsani, and Yaser P Fallah. Altruistic maneuver planning for cooperative autonomous vehicles using multi-agent advantage actor-critic. In *IEEE/CVF Conference on Computer Vision and Pattern Recognition, Workshop on Autonomous Driving: Perception, Prediction and Planning*, 2021.
33. Martin Treiber, Ansgar Hennecke, and Dirk Helbing. Congested traffic states in empirical observations and microscopic simulations. *Physical review E*, 62(2):1805, 2000.
34. Matteo Hessel, Joseph Modayil, Hado Van Hasselt, Tom Schaul, Georg Ostrovski, Will Dabney, Dan Horgan, Bilal Piot, Mohammad Azar, and David Silver. Rainbow: Combining improvements in deep reinforcement learning. In *AAAI Conference on Artificial Intelligence*, 2018.

35. Rusheng Zhang, Akihiro Ishikawa, Wenli Wang, Benjamin Striner, and Ozan K Tonguz. Using reinforcement learning with partial vehicle detection for intelligent traffic signal control. *IEEE Transactions on Intelligent Transportation Systems*, 22(1):404–415, 2020.
36. Martin Gregurić, Miroslav Vujić, Charalampos Alexopoulos, and Mladen Miletić. Application of deep reinforcement learning in traffic signal control: An overview and impact of open traffic data. *Applied Sciences*, 10(11):4011, 2020.
37. John DC Little and Stephen C Graves. Little’s law. In *Building intuition*, pages 81–100. Springer, 2008.
38. Volodymyr Mnih, Koray Kavukcuoglu, David Silver, Andrei A Rusu, Joel Veness, Marc G Bellemare, Alex Graves, Martin Riedmiller, Andreas K Fidjeland, Georg Ostrovski, et al. Human-level control through deep reinforcement learning. *nature*, 518(7540):529–533, 2015.
39. Tom Schaul, John Quan, Ioannis Antonoglou, and David Silver. Prioritized experience replay. In *International Conference on Learning Representations*, 2016.
40. Hado Van Hasselt, Arthur Guez, and David Silver. Deep reinforcement learning with double q-learning. In *AAAI Conference on Artificial Intelligence*, page 2094–2100, 2016.
41. Ziyu Wang, Tom Schaul, Matteo Hessel, Hado Hasselt, Marc Lanctot, and Nando Freitas. Dueling network architectures for deep reinforcement learning. In *International Conference on Machine Learning*, pages 1995–2003, 2016.
42. Marc G Bellemare, Will Dabney, and Rémi Munos. A distributional perspective on reinforcement learning. In *International Conference on Machine Learning*, pages 449–458, 2017.



43. Meire Fortunato, Mohammad Gheshlaghi Azar, Bilal Piot, Jacob Menick, Ian Osband, Alex Graves, Vlad Mnih, Remi Munos, Demis Hassabis, Olivier Pietquin, et al. Noisy networks for exploration. *International Conference on Learning Representations*, 2018.
44. Shangding Gu, Long Yang, Yali Du, Guang Chen, Florian Walter, Jun Wang, Yaodong Yang, and Alois Knoll. A review of safe reinforcement learning: Methods, theory and applications. *arXiv preprint arXiv:2205.10330*, 2022.

## Supplementary Materials

The supplementary materials include:

Text S1: Analysis of the Reward Function in Yan and Wu (13).

Fig. S1: Comparison between our hybrid reward and the reward function in Yan and Wu (13).

Fig. S2: The evaluation results at the intersection 449.

Fig. S3: The evaluation results at the intersection 332.

Fig. S4: The evaluation results at the intersection 334.

Fig. S5: The relationship between traffic demand, RV penetration rates and traffic congestion.

Fig. S6: Traffic light blackout experiments.

Fig. S7: RV ‘offline’ experiments.

Fig. S8: The two unseen intersections used in our testing.

Fig. S9: The evaluation results at unseen four leg intersection.

Fig. S10: The evaluation results at unseen three leg intersection.

Fig. S11: The illustration of the occupancy map.

Fig. S12: The number of conflict decisions during training and testing.

Tab. S1: The features of four main intersections (229, 449, 332, 334).

Tab. S2: The details of the two unseen intersections used in generalization experiments.

### Text S1 Analysis of the Reward Function in Yan and Wu (13)

In this part, we show why the reward function of the state-of-the-art technique by Yan and Wu (13) is difficult to scale to large-scale traffic scenarios.

The reward function by Yan and Wu (13) takes the format  $R_{Yan} = \text{outflow}(s_t, s_{t+1}) - \text{collision}(s_t, s_{t+1})$ , where  $\text{outflow}(s_t, s_{t+1})$  denotes the number of vehicles exiting the net-

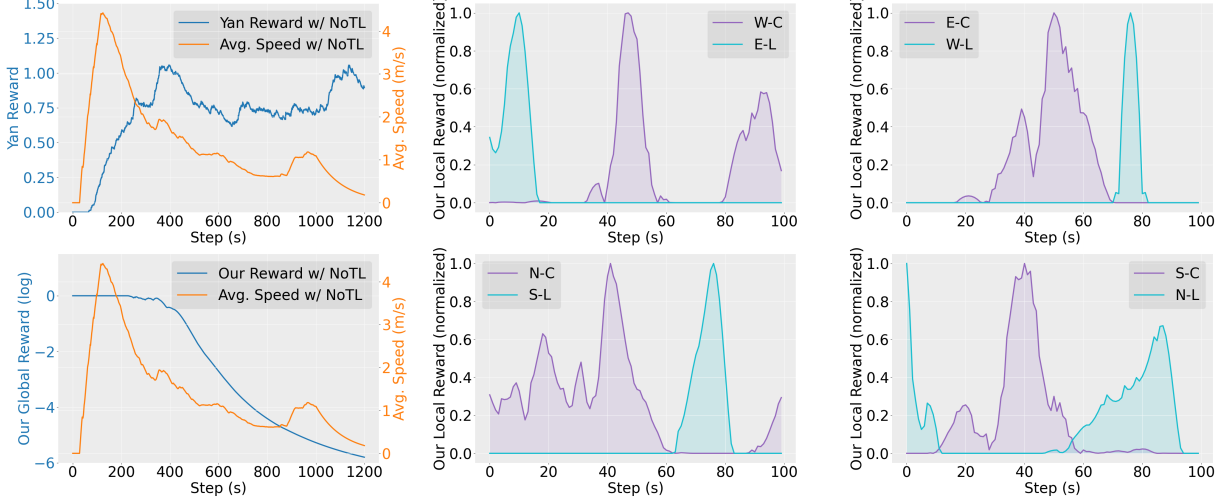


Figure S1: TOP-LEFT: Reward by Yan and Wu (13) calculated with the NoTL baseline. The average speed of all vehicles at the intersection is also plotted for comparison. The decreasing of the average speed indicates the form of congestion. As a result, Yan Reward does not reflect the intersection congestion timely. BOTTOM-LEFT: The accumulative global reward of ours, which responds to the intersection congestion swiftly. MIDDLE and RIGHT: the local reward of a pair of conflicting moving directions. The alternating patterns show the effectiveness of the local reward in enabling interchanges of traffic flows at the intersection.

work from  $t$  to  $t + 1$ , and  $\text{collision}(s_t, s_{t+1})$  is the number of collisions in the network from  $t$  to  $t + 1$ . We record this reward during the evaluation of the NoTL baseline to analyze its characteristics. The results are shown in TOP-LEFT and BOTTOM-LEFT of Fig. S1. As expected, for the NoTL baseline (with 100% HVs), congestion is formed at the intersection, which is reflected by the average speed of all vehicles decreasing to 0. However,  $R_{Yan}$  (Yan Reward) does not reflect the change of traffic conditions timely. This is because the outflow of a network is a delayed indicator: the congestion inside the intersection does not prohibit the vehicles that have already exited the intersection to continue contributing to the outflow. The delayed reward increases the difficulty of learning since an episode is likely to terminate due to the congestion before the reward eventually reflects it.

Intersection	Num. incoming lanes	Num. non-empty lanes	Traffic demand (v/h * lane)
229	21	19	694
449	19	18	620
332	18	17	662
334	16	14	515

Table S1: Intersection features. Among four intersections, 229 is the busiest one with the highest traffic demand (i.e., 694 vehicles per lane per hour) and the most non-empty lanes (i.e., 19).

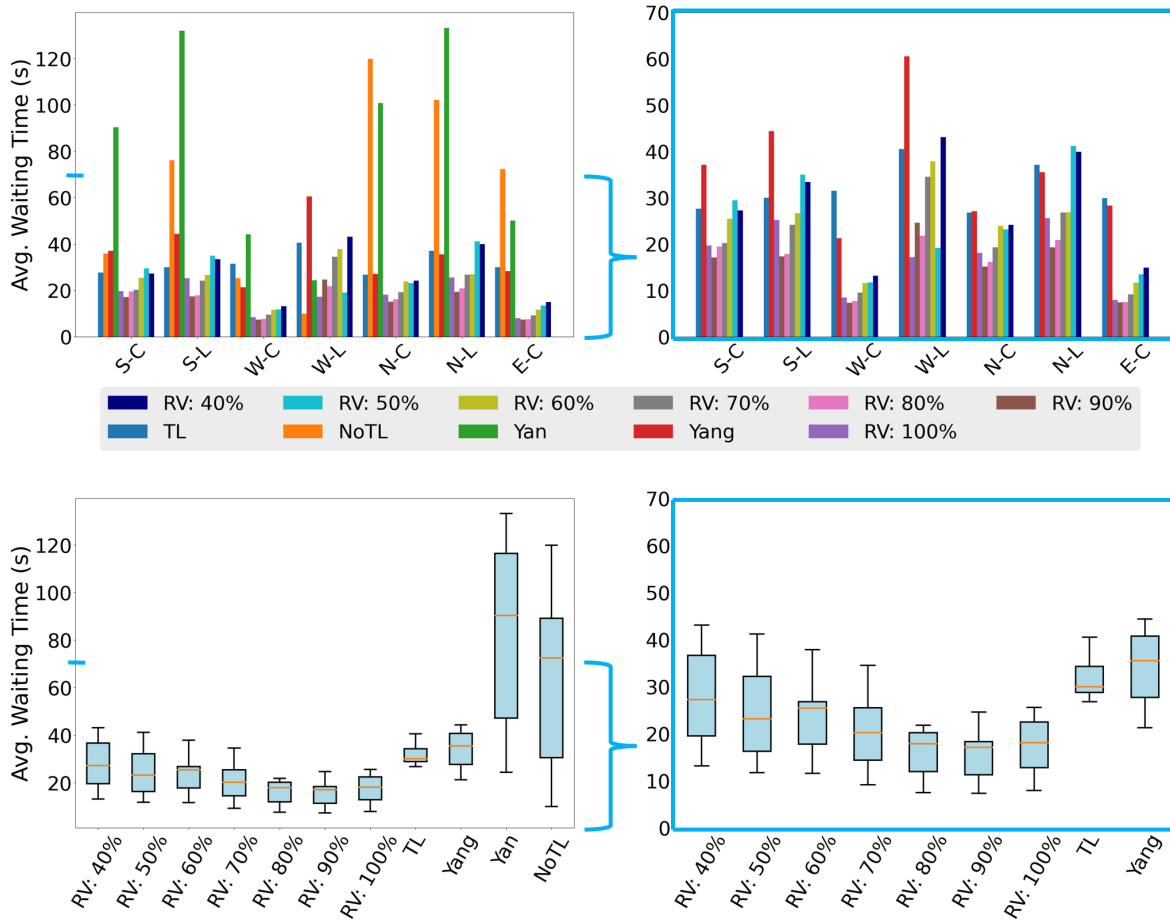


Figure S2: The overall results measured in average waiting time at the intersection 449. The RIGHT sub-figures are zoomed-in versions of the LEFT sub-figures by excluding NoTL and Yan. With 60% or more RVs, our method consistently outperforms all other baseline methods.

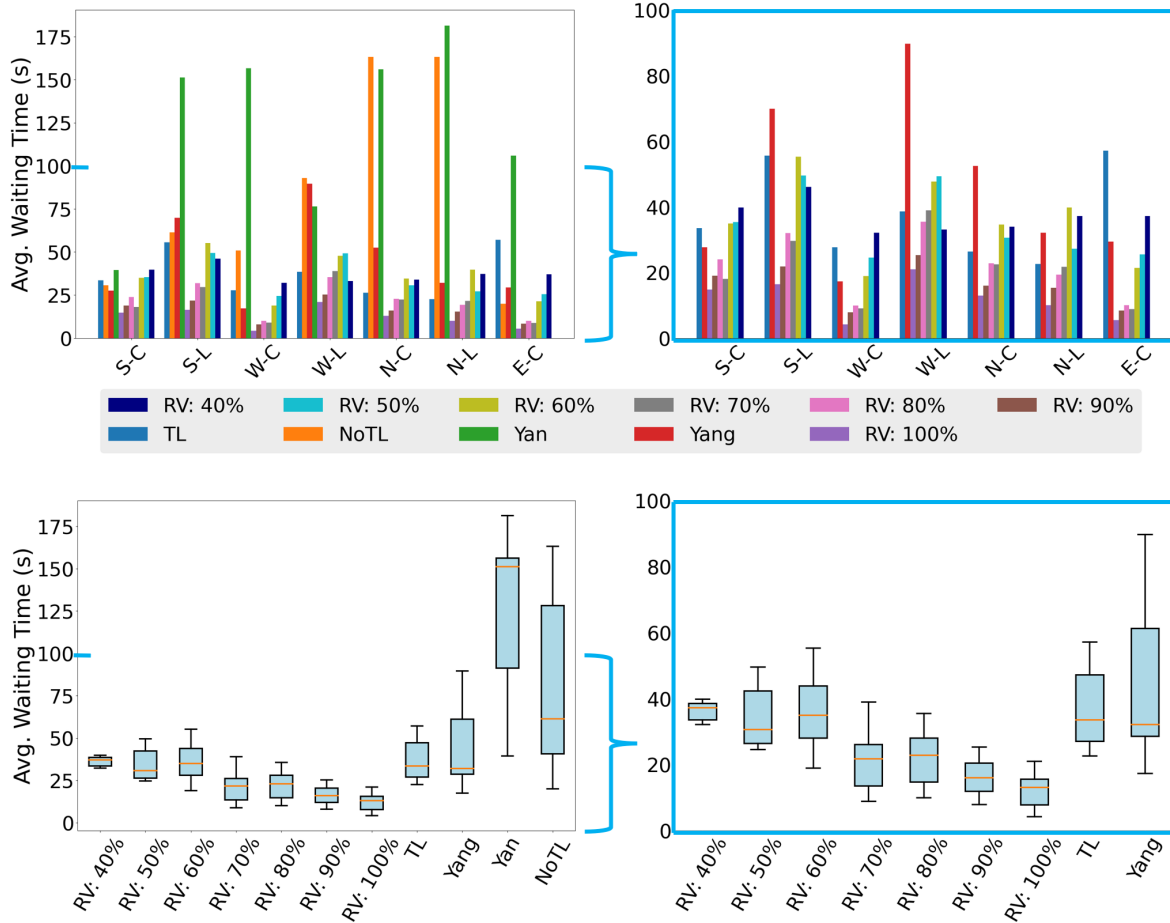


Figure S3: The overall results measured in average waiting time at the intersection 332. The RIGHT sub-figures are zoomed-in versions of the LEFT sub-figures by excluding NoTL and Yan. Generally speaking, NoTL and Yan do not perform very well. Our method starts to outperform TL and Yang when the RV penetration rate is 70% or higher.

Intersection	Topology	Num. lanes	Num. non-empty lanes	Traffic demand (v/h * lane)
140	four-legged	24	24	537
205	three-legged	10	10	700

Table S2: Details of the two unseen intersections used in our testing.

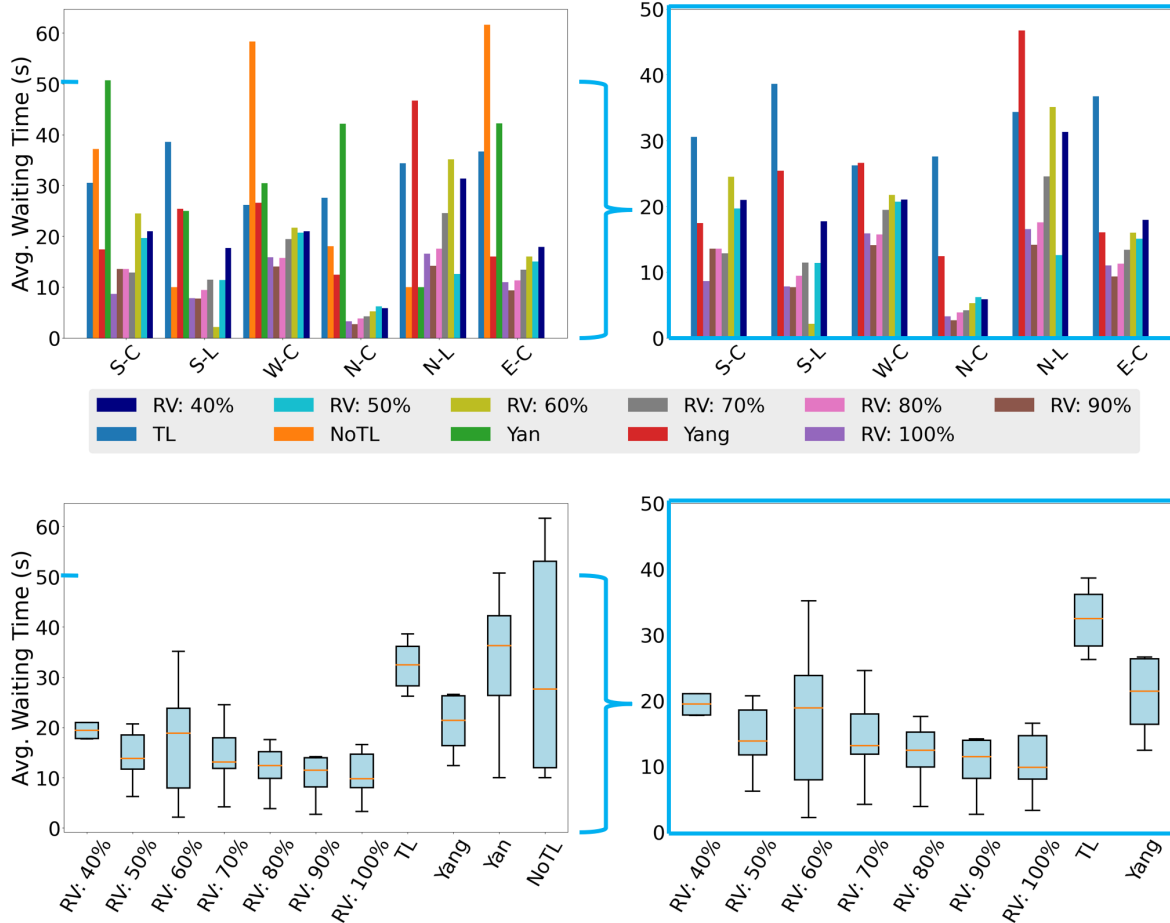


Figure S4: The overall results measured in average waiting time at the intersection 334. The RIGHT sub-figures are zoomed-in versions of the LEFT sub-figures by excluding NoTL and Yan. In general, our method with 50% RVs or more outperforms all four baselines.

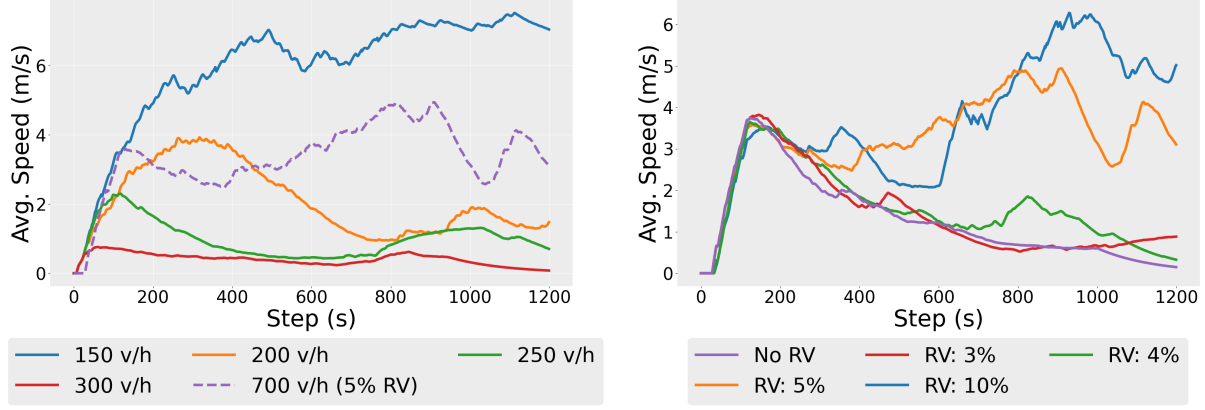


Figure S5: LEFT: The solid lines represent no traffic lights and no RVs. The congestion starts to form when the demand is over 200 v/h. The real-world demand denoted using the dash line, which is about 700 v/h, does not build congestion because 5% RVs are deployed in traffic. RIGHT: Analyzing the influence of low RV penetration rates on traffic. As a result, 5% is the minimum to prevent congestion. For both figures, the study subject is the intersection 229.

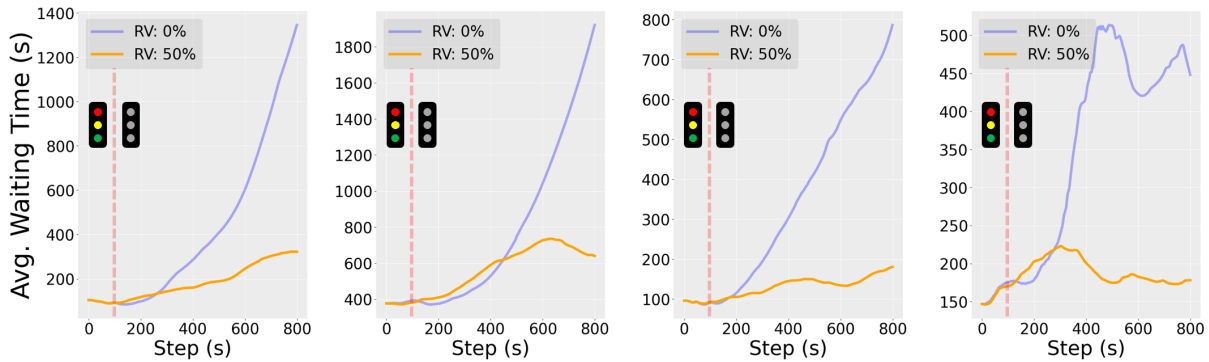


Figure S6: Blackout experiments. We simulate blackout events (traffic signals are off) at intersections 229, 332, 449, and 334 (from left to right) since the 100th step. Without any RV, a gridlock will form at the intersection causing the average waiting time of all vehicles to increase rapidly. In contrast, with 50% RVs, no gridlock is formed and the waiting times of all vehicles at the intersection remain low and stable.

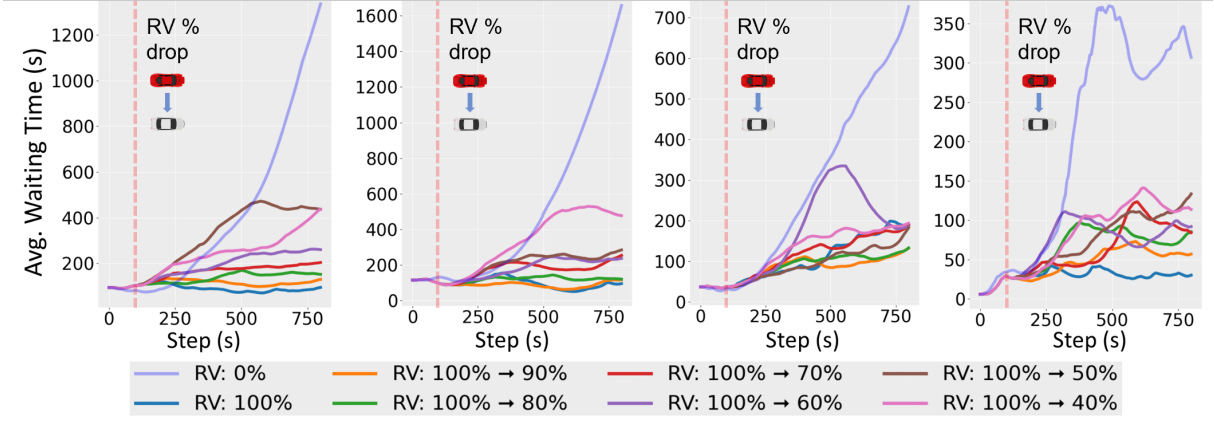


Figure S7: RV ‘offline’ experiments. The RV penetration rate drops from 100% to various percentages at intersections 229, 332, 449, and 334 (from left to right) since the 100th step. The ‘offline’ RVs are taken over by the IDM model. A pure HV scenario (100% HVs) is also included for comparison. As a result, even if the RV penetration rate reduces to 40%, our method can still maintain stable average waiting times of all vehicles at the intersection, reflecting no occurrence of gridlocks.



Figure S8: The two unseen intersections used in our testing (left is four-legged and right is three-legged).



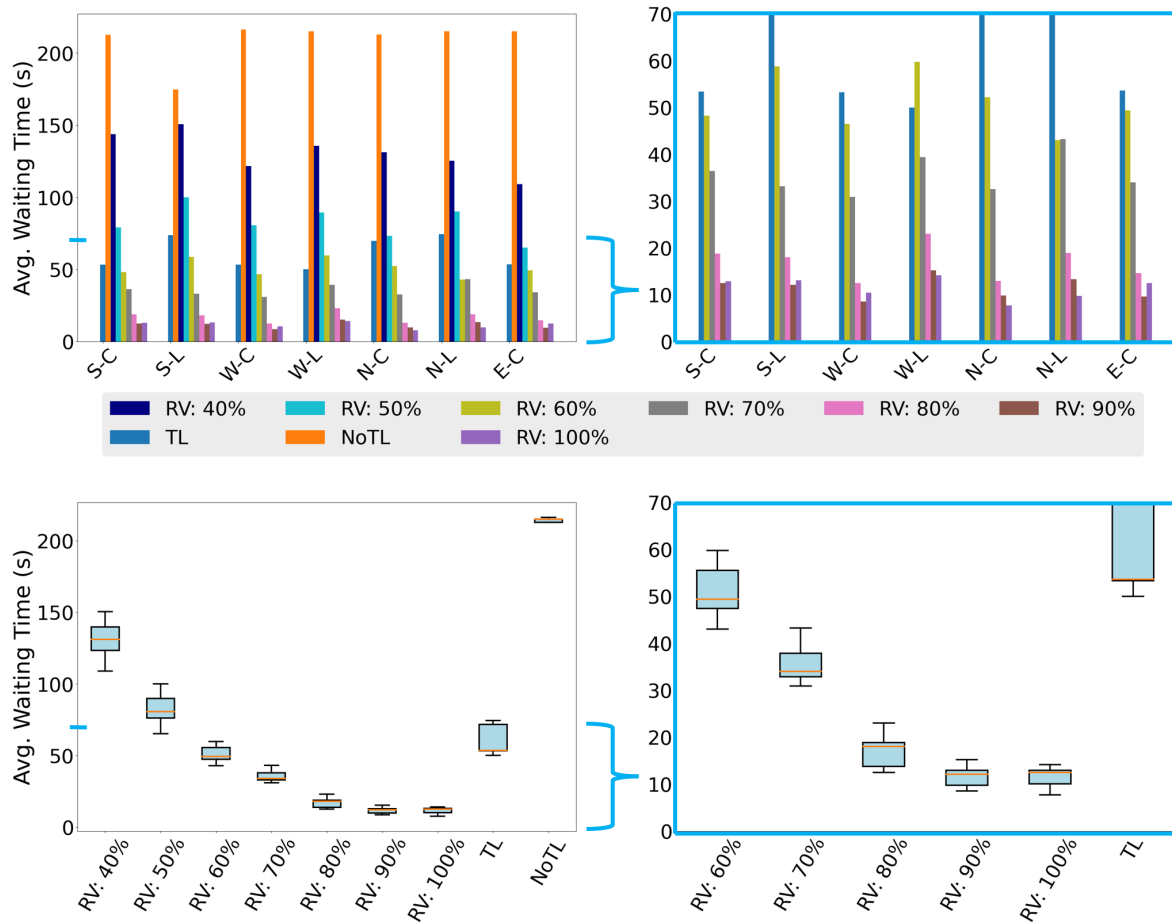


Figure S9: The overall results measured in average waiting time at the intersection 140 (unseen). The RIGHT sub-figures are zoomed-in versions of the LEFT sub-figures by excluding NoTL and RV percentages 40% and 50%. Starting from 60% RVs, our method beats the TL baseline. With 100% RVs, our method can reduce the average waiting time by  $\sim 80\%$  compared to TL.

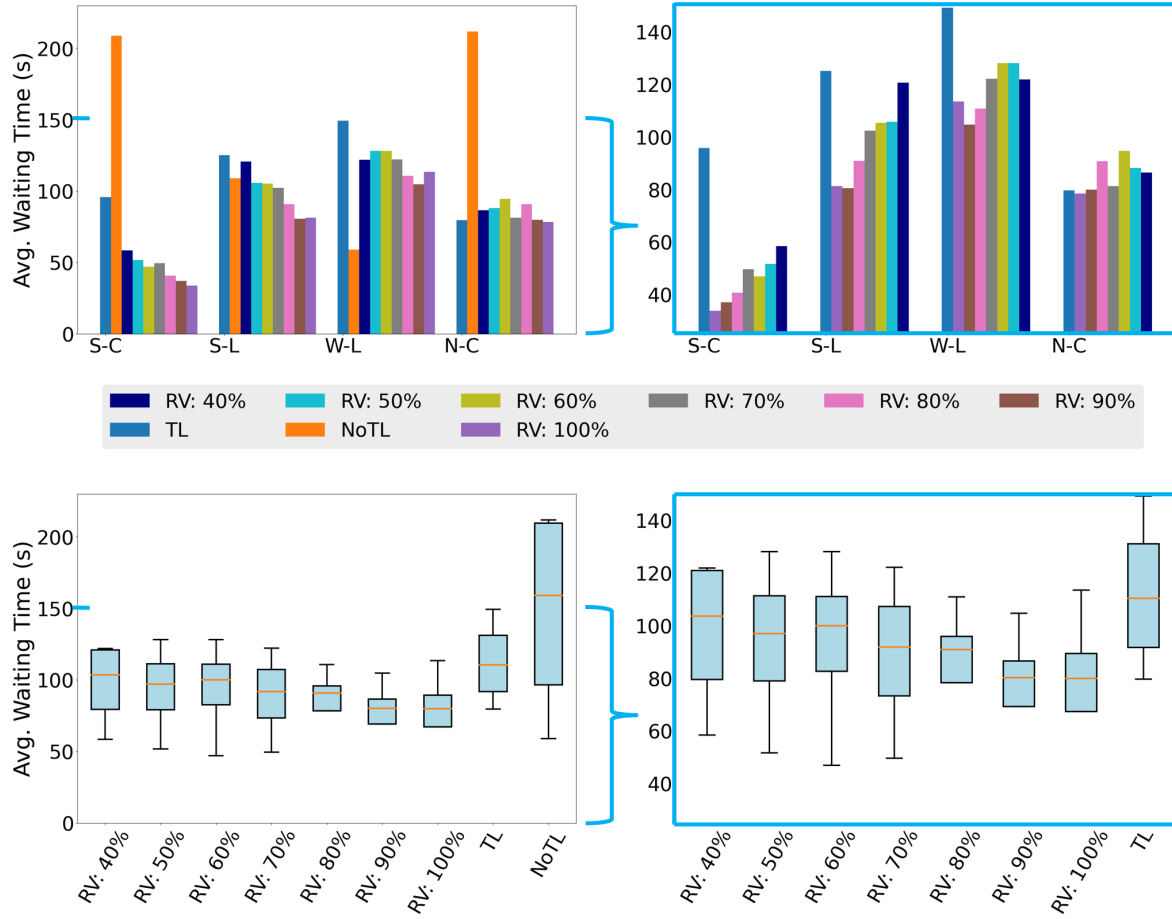


Figure S10: The overall results measured in average waiting time at the intersection 205 (unseen). This is a three-legged intersection and thus only four directions are shown. The RIGHT sub-figures are zoomed-in versions of the LEFT sub-figures by excluding NoTL. Our approach starts to outperform the TL baseline when RVs are 50% or more.

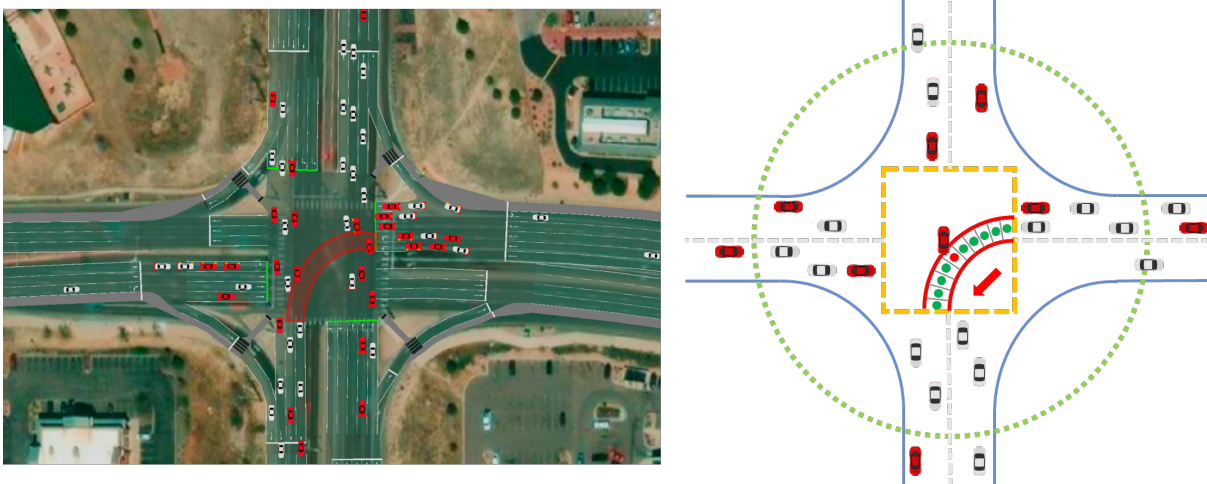


Figure S11: An illustration of the occupancy map along the moving direction W-L. The inner lanes are divided into 10 segments. Each segment has an associated binary label representing ‘free’ (green dot) or ‘occupied’ (red dot).

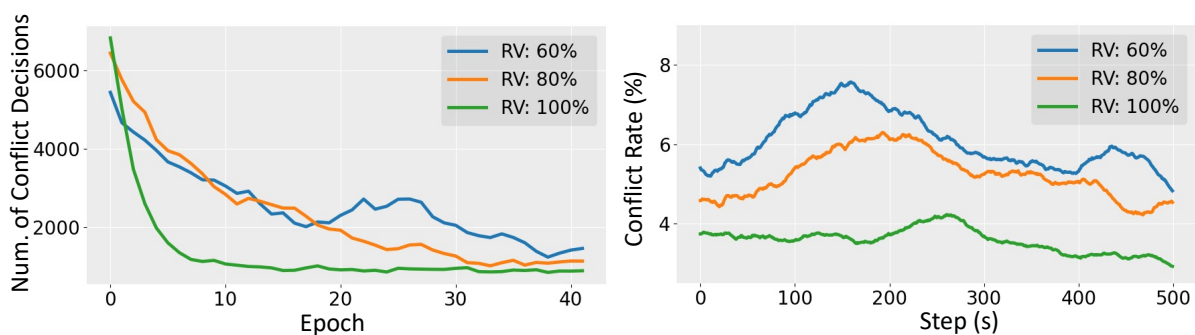


Figure S12: LEFT: The number of conflict decisions decreases as the learning progresses. For all three RV penetration rates, the trend stabilizes at a low level. RIGHT: The conflict rate (= num. of conflict decisions / num. of RVs within the control zone) is low for any RV penetration rate—around 5% for 60% RVs and 80% RVs, and close to 0 for 100% RVs.